 doi:10.20944/preprints202101.0313.v1

Article

Human Symmetry Uncertainty Detected by a Self-Organizing Neural Network Map

Birgitta Dresp-Langley[1]*, John M. Wandeto[2]

[1] ICube Lab UMR 7357 CNRS, Strasbourg University, FRANCE; birgitta.dresp@unistra.fr
[2] Department of Information Technology, Dedan Kimathi University of Technology, KENYA; john.wandeto@dkut.ac.ke
* Correspondence: birgitta.dresp@unistra.fr

Abstract: Symmetry in biological and physical systems is a product of self-organization driven by evolutionary processes, or mechanical systems under constraints. Symmetry-based feature extraction or representation by neural networks may unravel the most informative contents in large image databases. Despite significant achievements of artificial intelligence in recognition and classification of regular patterns, the problem of uncertainty remains a major challenge in ambiguous data. In this study, we present an artificial neural network that detects symmetry uncertainty states in human observers. To this end, we exploit a neural network metric in the output of a biologically inspired Self-Organizing Map, the Quantization Error (SOM-QE). Shape pairs with perfect geometric mirror symmetry but a non-homogenous appearance, caused by local variations in hue, saturation, or lightness within and/or across the shapes in a given pair produce, as shown here, longer choice RT for 'yes' responses relative to symmetry. These data are consistently mirrored by the variations in the SOM-QE from unsupervised neural network analysis of the same stimulus images. The neural network metric is thus capable of detecting and scaling human symmetry uncertainty in response to patterns. Such capacity is tightly linked to the metric's proven selectivity to local contrast and color variations in large and highly complex image data.

Keywords: symmetry; shape; local color; self-organized visual map; quantization error; SOM-QE; choice response time; human decision; uncertainty

1. Introduction

Symmetry in biological and physical systems is a product of self-organization [1] driven by evolutionary processes and/or mechanical systems under constraints. It conveys a basic feature to living objects, from molecules to animal bodies, or to physical forces acting in synergy to create symmetrical structures [1-6]. In pattern formation, perfect symmetry is a regularity within a pattern the two halves of which are mirror images of each other. In information theory and in particular human information processing [7-11], symmetry is considered an important carrier of information, detected universally by humans from an early age on [12,13]. Human symmetry detection [14, 15] in patterns or shapes involves visual and cognitive processes from lower to higher levels of functional organization [16-24]. Vertical mirror symmetry is a particularly salient form of visual symmetry [23-25], processed at early stages in human vision and producing greater or lesser detection reliability [23] depending on local features of the stimulus display with greater or lesser stimulus certainty. Shape symmetry is a visual property that attracts attention [18] and determines perceived volume [19-22] and perceptual salience [26] of objects represented in the two-dimensional image plane. Aesthetic judgment and choice preference [27,28] are influenced by symmetry, justifying biologically inspired models of symmetry perception in humans [29] under the light of the fact that symmetry is detected not only by primates but also by other species, such as insects, for example [30].

 doi:10.20944/preprints202101.0313.v1

Symmetry may be exploited in pattern detection and classification by neural networks, which may have to learn multiple copies of one and the same object representation displayed in different orientations. Encoding symmetry as a shape prior in the network can, therefore, help avoid redundant computation where the network has to learn to detect a same pattern or shape in multiple orientations [31]. Symmetry-based feature extraction and/or representation [32] by neural networks using deep learning can, for example, help discover the most informative representations in large image databases with only a minor amount of preprocessing [33]. However, despite significant achievements of artificial intelligence in recognition and classification of well-reproducible patterns, the problem of uncertainty still requires additional attention, especially in ambiguous data. An artificial neural network that detects uncertainty states where a human observer doubts about an image interpretation has been described previously for the case of MEG image data with significant ambiguity [34].

Here in this study, we present an artificial neural network that detects uncertainty states in human observers about shape symmetry. To this end, we exploit a neural network metric in the output of a biologically inspired Self-Organizing Map, the Quantization Error (SOM-QE) [35-44], which is a measure of output variance and quantifies the difference between neural network states at different stages of unsupervised image learning. In our previous studies, we demonstrated functional properties of the SOM-QE such as a sensitivity to the spatial extent, intensity, and sign or color of local image contrasts in unsupervised image classification by the neural network. The metric reliably detects the finest, clinically or functionally relevant variations in local image contrast contents [36-44], often invisible to the human eye [38,39,42-44]. Here it will be shown that the SOM-QE as a neural network state metric reliably captures, or correlates with, varying levels of human uncertainty in the detection of symmetry of shape pairs with varying local color contents. While all shape pairs present perfect geometrically defined vertical mirror symmetry, visual uncertainty about symmetry is introduced by systematic variations in color (hue) and or saturation of the local shape elements. Previous work using human two-alternative forced choice decision had shown that such color variations significantly influence perceived relative distance [45-48] in two-dimensional patterns. Here, psychophysically determined choice response times, previously shown to directly reflect stimulus uncertainty [49,50], are exploited as a measure of symmetry uncertainty in humans, where longer choice response times reflect a higher level of uncertainty.

2. Materials and Methods

Visual uncertainty associated with the symmetry of shape pairs was varied experimentally in a series of two-dimensional images showing shape pairs with perfect geometrical (vertical mirror) symmetry but varying color (hue and/or saturation) of local shape elements. To quantify human decision uncertainty, the images with the shape pairs were presented in random order on a computer screen to observers who had to decide as quickly as possible whether two shapes in a given images were symmetrical or not (*yes*/*no* procedure). The psychophysically measured choice response time was computed as measure of uncertainty. To test whether a biologically inspired Self-Organizing Map (SOM) reliably detects the different levels of human uncertainty reflected by the psychophysical response time variations, the same images where submitted to unsupervised neural network analysis to measure the Quantization Error in the SOM output (SOM-QE) after unsupervised learning.

2.1. Images and symmetry display

Images with colored mirror symmetric shape pairs, shown here for illustration in Figure 1, displayed on a medium grey (R=130, G=130, B=130) background covering a surface of 2560x1361 pixels were generated in *Photoshop 12* for visual presentation on a computer screen (EIZO COLOR EDGE CG 275W, 2560x1440 pixel resolution) connected to a DELL computer equipped with a high performance graphics card (NVIDIA). Color

Preprints (www.preprints.org) | NOT PEER-REVIEWED | Posted: 18 January 2021 doi:10.20944/preprints202101.0313.v1

and luminance calibration of the RGB channels of the monitor was performed using the appropriate Color Navigator self-calibration software, which was delivered with the screen and runs under Windows. Visual symmetry uncertainty in the shape pairs was varied by giving the local shape elements variable color appearance in terms of hue, lightness and saturation. Color parameters were selectively manipulated in Adobe RGB color space, the corresponding physical variations are here below given in Table 1.

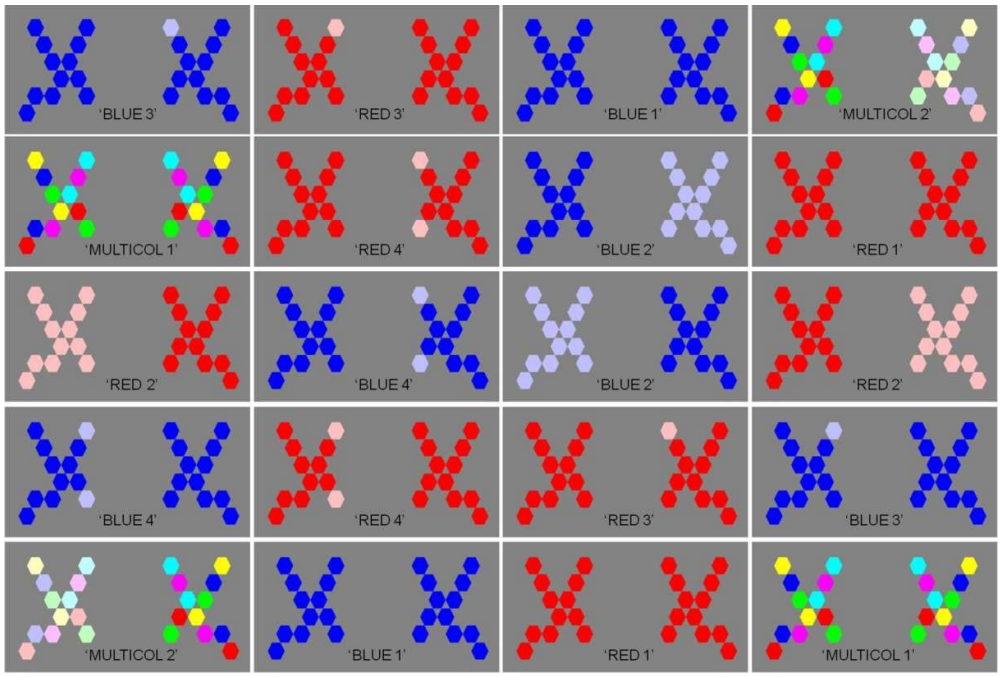

Figure 1. The test images with colored mirror symmetric shape pairs, displayed on a medium grey background. Visual symmetry uncertainty in the shape pairs was varied by giving local shape elements variable color appearance in terms of hue, lightness, and saturation.

Table 1. Local physical color parameters producing variations in pattern appearance.

	Color	Hue	Saturation	Lightness	R-G-B
"Strong"	BLUE	240	100	50	0-0-255
	RED	0	100	50	255-0-0
	GREEN	120	100	50	0-255-0
	MAGENTA	300	100	50	255-0-255
	YELLOW	60	100	50	
"Pale"	BLUE	180	95	50	10-250-250
	RED	0	100	87	255-190-190
	GREEN	120	100	87	190-255-190
	MAGENTA	300	25	87	255-190-255
	YELLOW	600	65	67	255-255-190

 doi:10.20944/preprints202101.0313.v1

2.2. Choice Response Time Test

In the test phase measuring human decision times, the 20 images were displayed in random order in two successively repeated test sessions per human observer. Tests were run a workstation consisting of a computer screen (EIZO COLOR EDGE CG 275W, 2560x1440 pixel resolution) connected to a DELL computer equipped with a high performance graphics card (NVIDIA). Fifteen healthy young individuals from a population of undergraduates and young professionals participated in the test phase. All participants had normal or corrected-to-normal visual acuity. In addition, the Ishihara plates [51] were used prior to individual testing to ensure that all of them also had normal color vision. The choice response tests were run in October and November 2019, and in conformity with the Helsinki Declaration for scientific experiments on human individuals. All the individuals provided informed consent to participate. Their identity is not revealed. The test procedure adheres to rules and regulations set by the ethics board of the corresponding author's host institution (CNRS) for response data collection from healthy human individuals in non-invasive psychophysical tasks, for which examination of the experimental protocol by a specific ethics committee is not mandatory. Each individual participant was comfortably seated in front of the computer at a distance of about 80 cm from the screen in a semi-dark room under *mesopic* viewing conditions, and adapted to surround light conditions for about five minutes. Participants were informed that images with two abstract patterns, one on the left and one on the right, would be shown on the screen in two separate sequences. The task instruction given to each of them was to: "decide as quickly as possible and as soon as an image comes up on the screen whether or not the two patterns in the given image appear to be symmetrical or not". A keyboard response had to be delivered by pressing '1' for '*yes*' or '2' for 'no'. Individuals had to maintain their index and middle fingers of their dominant hand ready on the numbers to be able to press a given key without any motor response delay. Each individual response choice was recorded and stored in a labeled data column of an excel file. The choice response time corresponds to the time between an image onset and the moment a response key is pressed. The response times associated with a 'yes' or 'no' decision were stored in a second labeled data column of the same excel file. As soon as a response was given, the current image disappeared from the screen, and 900 milliseconds later the next image was delivered. Image presentation and response data encoding were controlled by a program written in Python for Windows [52,53].

2.3. Neural Network (SOM) Analysis

The conceptual background and method of neural network analysis follows the same principle and protocol already described in our latest previous work on biological cell imaging data analysis by SOM [37,44]. It is described here again in full detail, for the benefit of the reader. The Self-Organizing Map is a an artificial neural network architecture that may be described formally as a nonlinear, ordered, smooth mapping of high-dimensional input data onto the elements of a regular, low-dimensional array [54]. It is assumed that the set of input variables is definable as a real vector x, of n-dimension. A parametric real vector m_i of n-dimension is associated with each element in the SOM. Vector m_i is a model and the SOM is therefore an array of models. Assuming a general distance measure between x and m_i denoted by $d(x,m_i)$, the map of an input vector x on the SOM array is defined as the array element m_c that matches best (smallest $d(x,m_i)$) with x. During the learning process, the input vector x is compared with all the m_i in order to identify m_c. The Euclidean distances $||x-m_i||$ define m_c. Models topographically close in the map up to a certain geometric distance, indicated by h_{ci}, will activate each other to learn something from their common input x. This results in a local relaxation or smoothing effect on the models in this neighborhood, which in continuous learning leads to global ordering. SOM learning is represented by the equation

$$m(t+1) = m_i(t) + \alpha(t)h_{ci}(t)[x(t) - m_i(t)] \quad (1)$$

where $t = 1,2,3\ldots$is an integer, the discrete-time coordinate, $h_{ci}(t)$ is the neighborhood function, a smoothing kernel defined over the map points which converges towards zero with time, $\alpha(t)$is the learning rate, which also converges towards zero with time and affects the amount of learning in each model. At the end of the *winner-take-all* learning process in the SOM, each image input vector x becomes associated to its best matching model on the map m_c. The difference between x and m_c, $||x-m_c||$, is a measure of how close the final SOM value is to the original input value and is reflected by the quantization error, QE. The average QE of of all x (X) in an image is given by:

$$QE = 1/N \sum_{i=1}^{N} \|X_i - m_{c_i}\| \quad (2)$$

where N is the number of input vectors x in the image. The final weights of the SOM are defined by a three dimensional output vector space representing each R, G, and B channel. The magnitude as well as the direction of change in any of these from one image to another is reliably reflected by changes in the QE. The SOM training process consisted of 1 000 iterations. The SOM was a two-dimensional rectangular map of 4 by 4 nodes, hence capable of creating 16 models of observation from the data. The spatial locations, or coordinates, of each of the 16 models or domains, placed at different locations on the map, exhibit characteristics that make each one different from all the others. When a new input signal is presented to the map, the models compete and the winner will be the model the features of which most closely resemble those of the input signal. The input signal will thus be classified or grouped in one of models. Each model or domain acts like a separate decoder for the same input, i.e. independently interprets the information carried by a new input. The input is represented as a mathematical vector of the same format as that of the models in the map. Therefore, it is the presence or absence of an active response at a specific map location and not so much the exact input-output signal transformation or magnitude of the response that provides the interpretation of the input. To obtain the initial values for the map size, a trial-and-error process was implemented. Map sizes larger than 4 by 4 produced observations where some models ended up empty, which meant that these models did not attract any input by the end of the training. As a consequence, 16 models were sufficient to represent all the fine structures in the image data. Neighborhood distance and learning rate were constant at 1.2 and 0.2 respectively. These values were obtained through the trial-and-error method after testing the quality of the first guess, which is directly determined by the value of the resulting quantization error ; the lower this value, the better the first guess. It is worthwhile pointing out that the models were initialized by randomly picking vectors from the training image, called here the "original image". This allows the SOM to work on the original data without any prior assumptions about a level of organization within the data. This, however, requires to start with a wider neighborhood function and a bigger learning-rate factor than in procedures where initial values for model vectors are pre-selected [55]. The approach is economical in terms of computation times, which constitutes one of its major advantages for rapid change/no change detection on the basis of large datasets. The 20 images here were fed into a single SOM. The training image for the SOM prior to further input can be any of these. After unsupervised *winner-takes-all* SOM learning, the SOM-QE output was written into a data file. Further steps generate output plots of SOM-QE, where each output value is associated with the corresponding input image. The output data are then plotted in increasing/decreasing orders of SOM-QE magnitude as a function of the corresponding image variations (automatic image classification). The computation time of SOM analysis of each of the 20 images was about two seconds per image. The code used for implementing the SOM-QE is available online at:
https://www.researchgate.net/publication/330500541_Self-organizing_map-based_quantization_error_from_images

Preprints (www.preprints.org) | NOT PEER-REVIEWED | Posted: 18 January 2021 doi:10.20944/preprints202101.0313.v1

3. Results

With 20 images per individual session, two successive sessions per participant, and 15 participants, a total of 600 choice response time data were recorded. A shape pair corresponding to a single factor level relative to shape appearance and color was presented twice in a session with 20 images to allow for left and right hand side presentation of a given appearance factor level in the shape pairs. The labels of the individual factor level associated with each shape pair are given in Figure 1. With two repeated sessions per participants, we have four individual response time data for each single factor level. All data analyses relative to choice response times were run on the 15 average response times for each factor level from the 15 participants. These data are made available here in Table S1 of the Supplementary Materials Section.

Since all shape pairs in all the images were mirror-symmetric, *'no'* responses occurred only very rarely in the experiment (17 of the 600 recorded choice responses signaled *'no'*, which corresponds to less than three percent of the total number of observations), as would be expected. In these rare cases, only the choice response times corresponding to a *'yes'* among the four responses recorded for a given factor level were used for computing the average. In terms of operational factor levels in the Cartesian experimental design plan, we have four levels (1,2,3,4) of a factor termed *'Appearance'* (A_4) associated with the colors BLUE and RED, and two levels (1,2) of *'Appearance'* (A_2) associated with the multiple color case termed MULTICOL here. The three color conditions, blue, red, and multicolor, describe three operational levels of a second factor termed *'Color'* (C_3) herein. In a first step, two separate two-way analyses of variance (ANOVA) were run to test for significant effects of the factors *'Appearance'* and *'Color'*. The first ANOVA compares between four levels of *'Appearance'* (1,2,3,4) in two levels (BLUE,RED) of the *'Color'* factor. The second ANOVA compares between two levels of *'Appearance'* in three levels (BLUE, RED, MULTICOL) of the *'Color'* factor.

3.1. Two-way ANOVA on choice response times

3.1.1. $A_4 \times C_2 \times 15$

This analysis corresponds to a Cartesian analysis plan $A_4 \times C_2 \times 15$, with four levels (1,2,3,4) of the '*Appearance*' factor and two levels (BLUE,RED) of the *'Color'* factor on the 15 individual average response times (RT), yielding a total number (N-1) of 119 degrees of freedom (DF). The results from this analysis are shown here below in the top part of Table 2.

Table 2. Results from the two-way analyses of variance with factor specific degrees of freedom (DF), the corresponding F statistics, and their associated probability limits (*p*).

	Factor	DF	F	*p*
1st 2-way ANOVA	APPEARANCE	3	68.42	<.001
	COLOR	1	.012	<.914 NS
	INTERACTION	3	5.37	<.01
2nd 2-way ANOVA	APPEARANCE	1	8.20	<.01
	COLOR	2	123.56	<.001
	INTERACTION	2	.564	<.57 NS

Preprints (www.preprints.org) | NOT PEER-REVIEWED | Posted: 18 January 2021 doi:10.20944/preprints202101.0313.v1

The results of this analysis signal a statistically significant effect of the *'Appearance'* factor on the average RT and a statistically significant interaction between the *'Appearance'* and the *'Color'* factor for the cases BLUE and RED. A statistically significant effect 'Color' independent of 'Appearance' is not observed, leading to conclude that either of these two colors produced similar effects on RT relative to shape symmetry when their appearance is modified. This holds with the exception for statistical comparison between BLUE3 and BLUE4, which is the only one that is not significant here, as revealed by the *post-hoc* comparison (Holm-Sidak) between these two factor levels (t(1,1) = .32, p<.75 NS). The effects can be appreciated further by looking at the effect sizes for the different conditions, which are visualized further here in the Figures 2 and 3.

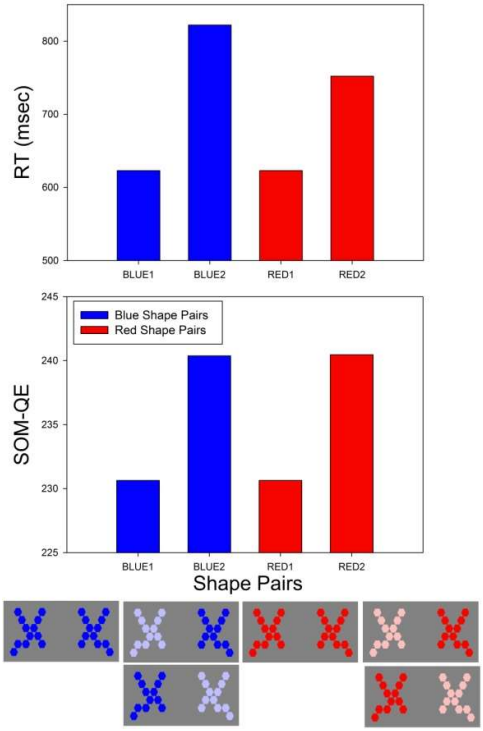

Figure 2. Statistically significant differences in average RT (top) for the comparison between BLUE and RED shape pairs with appearance levels 1 and 2. The corresponding SOM-QE values (bottom) from the neural network analysis are plotted in the graph below.

3.1.2. A_2 x C_3 x 15

This analysis corresponds to a Cartesian analysis plan *A_2 x C_3 x 15*, with two levels (1,2) of the *'Appearance'* factor and three levels (BLUE,RED,MULTICOL) of the *'Color'* factor on the 15 individual average response times (RT), yielding a total number (N-1) of 89 degrees of freedom. The results from this analysis are shown here above in the bottom part of Table 2. They signal a statistically significant effect of the *'Appearance'* factor on the average RT and a statistically significant effect of the *'Color'* factor. A statistically significant interaction is not observed here. Statistical *post-hoc* comparisons (*Holm-Sidak*) reveal statistically significant differences between the factor levels MULTICOL and RED (t(1,1) = 14.44, p<.001) and between the factor levels MULTICOL and BLUE (t(1,1) = 12.60, p<.001), but not, as could be expected from the previous ANOVA, between the factor levels RED and BLUE (t(1,1) = 1.84, p<.09 NS). The 'Color' effect here is reflected by the observation that shape pairs with multiple color elements yield significantly longer symmetry related RT compared with shape pairs composed of any of the two single col-

 doi:10.20944/preprints202101.0313.v1

ors here. This effect can be appreciated further by looking at the effect sizes for the different comparisons, which are visualized further below here in Figure 4.

3.2. RT effect sizes

The effect sizes, in terms of differences between means, that correspond to significant statistical differences signaled by two-way ANOVA were plotted graphically, and are shown in the top graph in Figure 2 here above, and in the top graphs in Figures 3 and 4 here below along with the corresponding shape pairs that produced the results. The graphs show clearly that shape pairs with non-homogenous appearance, i.e. local variations in hue, saturation, or lightness within and/or across shapes in a given pair, produce longer choice RT for *'yes'* responses relative to shape symmetry.

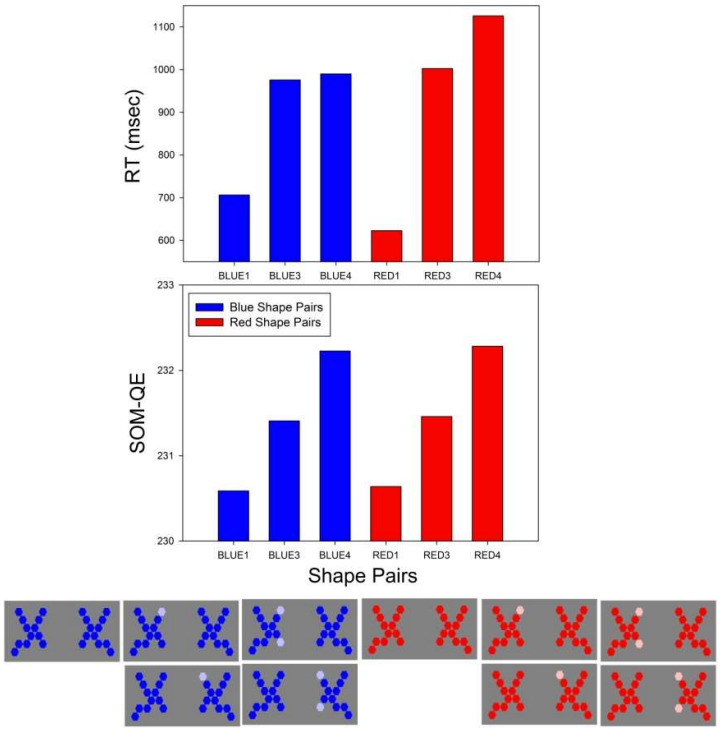

Figure 3. Statistically significant differences in average RT (top) for the comparison between BLUE and RED shape pairs with appearance levels 1, 3 and 4. The corresponding SOM-QE values (bottom) from the neural network analysis are plotted in the graph below. The difference in average RT between BLUE3 and BLUE4 is the only one here that is not statistically significant (see paragraph 3.1.1.).

3.3. SOM-QE effect sizes

The SOM-QE metrics from the unsupervised neural network analysis of the test images were also plotted graphically and are displayed in the bottom graphs of Figures 2, 3, and 4. The graphs show clearly that the magnitudes of the SOM-QE from the neural network analysis consistently mirror the observed magnitudes of average choice RT for *'yes'* responses relative to shape symmetry produced by shape pairs with varying appearance in terms of local variations in hue, saturation, or lightness within and/or across shapes in a given pair.

Preprints (www.preprints.org) | NOT PEER-REVIEWED | Posted: 18 January 2021 doi:10.20944/preprints202101.0313.v1

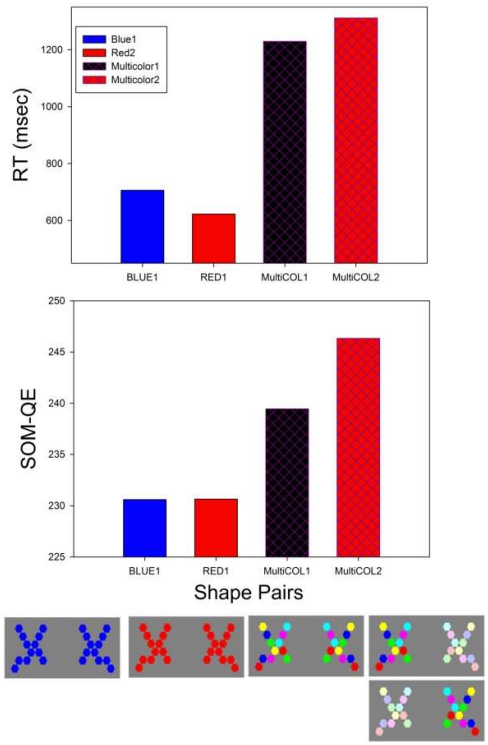

Figure 4. Differences in average RT (top) for the comparison between BLUE and RED shape pairs with appearance level 1 and the multicolored MULTICOL shape pairs with appearance levels 1 and 2. The differences between BLUE and RED shape pairs of any appearance level are not statistically significant (see paragraph 3.1.1.). The differences between image conditions BLUE1 or RED1 and MULTICOL1 and between BLUE2 or RED2 and MULTICOL2 are highly significant, as is the difference between MULTICOL1 and MULTICOL2 (see paragraph 3.1.2.). The corresponding SOM-QE values (bottom) from the neural network analysis are plotted in the graph below.

3.4. Linear regression analyses

The results from the previous analyses show that the average choice RT for *'yes'* responses relative to shape symmetry, produced by shape pairs with varying appearance in terms of local variations in hue, saturation, or lightness within and/or across shapes in a given pair, produce significant variations consistent with variations in decisional uncertainty about the mirror symmetry of the shapes in a pair. The higher the variability in hue, saturation or lightness of single shape elements, the longer the RT for 'yes" hence the higher the stimulus uncertainty for 'symmetry'. Indeed, the longest choice RT for *'yes'* responses relative to shape symmetry is produced by the shape pairs MULTICOL1 and MULTICOL2. To bring the tight link between variations in RT reflecting different levels of human uncertainty and the variations in the SOM-QE metric from the neural network analyses, we performed a linear regression analysis on the RT data for shape pairs with varying levels of appearance in BLUE, RED and MULTICOL shapes, and a linear regression analysis on the SOM-QE data for exactly the same shape pairs. The results from these analyses are plotted here below in Figure 5. The linear regressions coefficents (R2) are provided in the graph for each analysis. It is shown that RT for *'yes'* responses relative to shape symmetry and the SOM-QE as a function of the same shape variations follow highly similar and signficant linear trends.

Preprints (www.preprints.org) | NOT PEER-REVIEWED | Posted: 18 January 2021 doi:10.20944/preprints202101.0313.v1

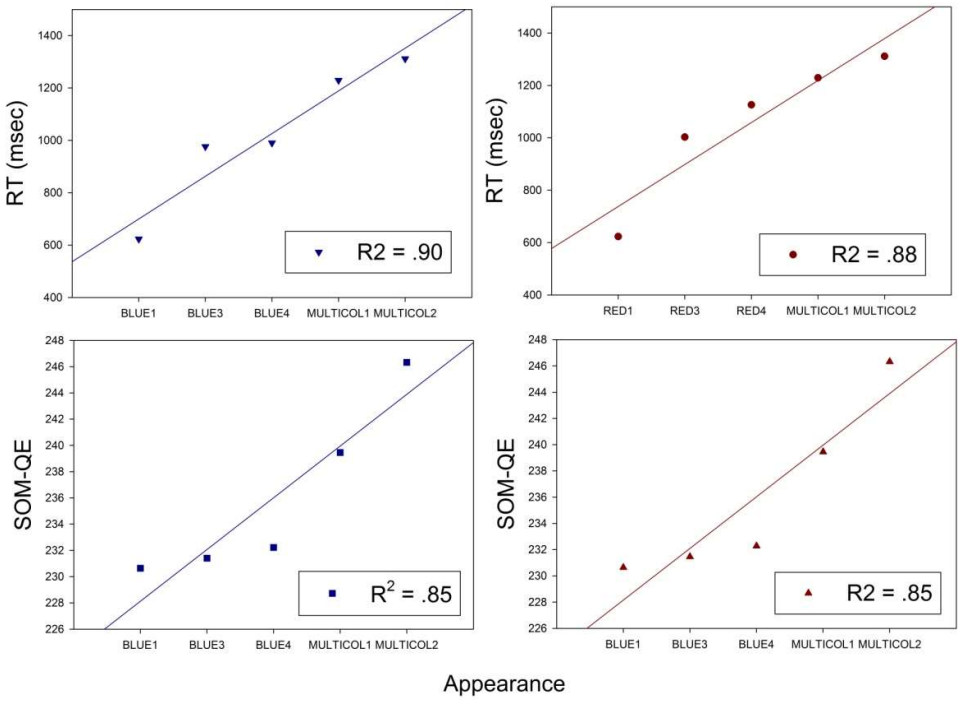

Figure 5. The tight link between variations in RT reflecting different levels of human uncertainty and the variations in the SOM-QE metric from the neural network analyses is brought to the fore here under the light of linear regression analysis on the RT data for shape pairs with varying levels of appearance in BLUE, RED and MULTICOL shapes, and linear regression analysis on the SOM-QE data for exactly the same shape pairs.

4. Discussion

It is shown here that mirror symmetric shape pairs with a non-homogenous appearance, caused by local variations in hue, saturation, or lightness within and/or across shapes in a given pair, produce longer choice RT for *'yes'* responses relative to the shape symmetry. The variations in average choice RT for *'yes'* responses are consistent with variations in human symmetry uncertainty [49,50]. The higher the variability in hue, saturation or lightness of single shape elements, the longer the RT for 'yes", i.e. the higher the stimulus uncertainty for 'symmetry'. As shown here, the variations in RT are consistently mirrored by the variations in the SOM-QE from the unsupervised neural network analysis of the same stimulus images. This provides further data showing that artificial neural networks are capable of detecting human uncertainty in perceptual judgment tasks [34]. The capability to the SOM-QE to capture such uncertainty in human choice responses to the symmetry of shapes with local variations in color parameters is tightly linked to the proven selectivity of this neural network metric to local contrast and color variations in large variety of complex image data [36-44]. Here, the metric is revealed as a measure of both variance in the image input data, and uncertainty in specific human decisions in response to such data. The neural network metric captures the effects of local color contrast [56] on symmetry saliency in cases where pure shape geometry signals perfect mirror symmetry. This unambiguously shows that visual parameters beyond stimulus geometry [57-60] influence what has previously been termed the "symmetry of things in a thing". Such local, non-geometrically determined effects on perceived shape symmetry have potentially important implications for image-guided human precision tasks [61,62], now more and more often assisted by neural network-driven image analysis

[32,33]. From a general functional viewpoint, the fact that local variations in hue, saturation, or lightness in geometrically perfect mirror symmetric shapes significantly increase human symmetry uncertainty by delaying conscious choice response times [49,57] is consistent with current theory invoking interactions between low-level visual and higher level cognitive mechanisms of integration [57,63]. In humans, the explicit and fully conscious detection of symmetry in choice response tasks involves integration of information beyond local information through brain networks with neurons displaying larger receptive field areas and a massive amount of lateral connectivity [64,65].

Supplementary Materials: Table S1: AverageResponseTimeData15Subjects.xls

Author Contributions: Conceptualization, B.D.L.; methodology, B.D.L., J.M.W.; software, J.M.W.; validation, B.D.L., J.M.W.; formal analysis, B.D.L, J.M.W.; investigation, B.D.L., J.M.W.; resources, B.D.L.; data curation, B.D.L., J.M.W.; writing—original draft preparation, B.D.L., J.M.W.; writing—review and editing, B.D.L., J.M.W.; visualization, B.D.L. All authors have read and agreed to the published version of the manuscript.

Funding: This research received no external funding.

Institutional Review Board Statement: The study was conducted according to the guidelines of the Declaration of Helsinki. All the individuals provided informed consent to participate. Their identity is not revealed. The test procedure fully adheres to rules and regulations set by the ethics board of the corresponding author's host institution (CNRS) for response data collection from healthy human individuals in non-invasive psychophysical choice response tasks, for which examination of the experimental protocol by a specific ethics committee is not mandatory. Ethical review and approval were, as a consequence, waived for this study.

Informed Consent Statement: Informed consent was obtained from all subjects involved in the study.

Data Availability Statement: All data exploited here are made available in this publication.

Acknowledgments: Material support from the CNRS is gratefully acknowledged.

Conflicts of Interest: The authors declare no conflict of interest

References

1. Schweisguth, F.; Corson, F. Self-Organization in Pattern Formation. Dev Cell, 2019, 49(5), 659-677.
2. Carroll, SB. Chance and necessity: the evolution of morphological complexity and diversity. Nature, 2001, 409, 1102–1109.
3. García-Bellido, A. Symmetries throughout organic evolution. Proc Natl Acad Sci U S A, 1996, 93, 14229–14232.
4. Groves, J. T. The physical chemistry of membrane curvature. *Nature Chemical Biology*, 2009, 5, 783-784.
5. Hatzakis, N. S.; Bhatia, VK.; Larsen, J.; Madsen,K.L.; Bolinger, P.Y.; Kunding, A.H.; Castillo, J.; Gether, U.; Hedegård, P.; Stamou, D. How curved membranes recruit amphipathic helices and protein anchoring motifs. *Nature Chemical Biology*, 2009, 5, 835-841.
6. Holló, G. Demystification of animal symmetry: symmetry is a response to mechanical forces. Biol Direct, 2017,12(1), article11.
7. Mach, E. *On Symmetry*, In Popular Scientific Lectures, 1893; Lasalle: Open Court Publishing.
8. Arnheim, R. *Visual Thinking,* 1969, University of California Press.
9. Deregowski, J. B. Symmetry, Gestalt and information theory. *Quarterly Journal of Experimental Psychology*, 1971, 23, 381-385.
10. Eisenman, R. Complexity–simplicity: I. Preference for symmetry and rejection of complexity. *Psychonomic Science*, 1967, 8, 169-170.

11. Eisenman, R.; Rappaport, J. Complexity preference and semantic differential ratings of complexity-simplicity and symmetry-asymmetry. *Psychonomic Science*, 1967, 7, 147–148.
12. Deregowski, J. B. The role of symmetry in pattern reproduction by Zambian children. *Journal of Cross-Cultural Psychology*, 1972, 3, 303–307.
13. Amir, O.; Biederman, I.; Hayworth, K.J. Sensitivity to non-accidental properties across various shape dimensions. *Vision Research,* 62, 35-43.
14. Bahnsen, P. Eine Untersuchung über Symmetrie und Asymmetrie bei visuellen Wahrnehmungen. *Zeitschrift für Psychologie*, 1928, 108, 129–154.
15. Wagemans, J. Characteristics and models of human symmetry detection. *Trends in Cognitive Sciences*, 1997**,** 9, 346-352.
16. Sweeny, T. D.; Grabowecky, M.; Kim, Y. J.; Suzuki, S. Internal curvature signal and noise in low- and high-level vision. *Journal of Neurophysiology*, 2011, 105, 1236-1257.
17. Wilson H. R.; Wilkinson F. Symmetry perception: A novel approach for biological shapes. *VisionResearch*, 2002, 42, 589–597.
18. Baylis, G.C.; Driver, J. Perception of symmetry and repetition within and across visual shapes: Part-descriptions and object-based attention. *Vis. Cognit.* 2001, *8*, 163–196.
19. Michaux, A.; Kumar, V.; Jayadevan, V.; Delp, E.; Pizlo, Z. Binocular 3D Object Recovery Using a Symmetry Prior. *Symmetry*, 2017, *9*, 64.
20. Jayadevan, V.; Sawada, T.; Delp, E.; Pizlo, Z. Perception of 3D Symmetrical and Nearly Symmetrical Shapes. *Symmetry*, 2018, *10*, 344.
21. Li, Y.; Sawada, T.; Shi, Y.; Steinman, R.M.; Pizlo, Z. Symmetry is the *sine qua non* of shape. In: S. Dickinson and Z. Pizlo (Eds.), Shape perception in human and computer vision, 2013, London, Springer (pp.21-40).
22. Pizlo, Z.; Sawada, T.; Li, Y.; Kropatsch, W.G.; Steinman, R.M. (2010) New approach to the perception of 3D shape based on veridicality, complexity, symmetry and volume: a mini-review. *Vision Research*, **50**, 1-11.
23. Barlow, H. B.; Reeves, B. C.The versatility and absolute efficiency of detecting mirror symmetry in random dot displays. *Vision Research*, 1979, 19, 783–793.
24. Barrett, B. T.; Whitaker, D.; McGraw, P. V.; Herbert, A. M. Discriminating mirror symmetry in foveal and extra-foveal vision. *Vision Research*, 1999, 39, 3737–3744.
25. Machilsen, B.; Pauwels, M.;Wagemans, J. The role of vertical mirror symmetry in visual shape perception. *Journal of Vision*, 2009, 9(11).
26. Dresp-Langley, B. Bilateral Symmetry Strengthens the Perceptual Salience of Figure against Ground. *Symmetry,* 2019, *11*, 225.
27. Dresp-Langley, B. Affine Geometry, Visual Sensation, and Preference for Symmetry of Things in a Thing. *Symmetry,* 2016, *8*, 127.
28. Sabatelli, H.; Lawandow, A.; Kopra, A. R. Asymmetry, symmetry and beauty. *Symmetry*, 2010, 2, 1591-1624.
29. Poirier, F.J.A.M.; Wilson, H.R. A biologically plausible model of human shape symmetry perception. *J. Vis.* 2010, *10*, 1–16.
30. Giurfa, M.; Eichmann, B.; Menzl, R. Symmetry perception in an insect. *Nature*, 1996, 382, 458–461.
31. Krippendorf, S.; Syvaeri, M. *Mach. Learn. Sci. Technol.* 2021, 2, article 015010.
32. Toureau, V.; Bibiloni, P., Talavera-Martínez, L., González-Hidalgo, M. Automatic Detection of Symmetry in Dermoscopic Images Based on Shape and Texture. *Information Processing and Management of Uncertainty in Knowledge-Based Systems*, 2020, 1237, 625-636.
33. Shen, D.; Wu, G.; Suk, HI. Deep Learning in Medical Image Analysis. *Annu Rev Biomed Eng*, 2017, 19, 221-248.

34. Hramov, A.E.; Frolov, N.S.; Maksimenko, V.A.; Makarov, V.V.; Koronovskii, A.A.; J.Garcia-Prieto, J.; Antón-Toro, L.F.; Maestú, F.; Pisarchik, A.N. Artificial neural network detects human uncertainty, *Chaos*, 2018, 28, article 033607.
35. Dresp-Langley, B. Seven Properties of Self-Organization in the Human Brain. *Big Data Cogn. Comput.*, 2020, *4*, 10.
36. Wandeto J.M.; Dresp-Langley, B. Ultrafast automatic classification of SEM image sets showing CD4 + cells with varying extent of HIV virion infection. *7ièmes Journées de la Fédération de Médecine Translationnelle de l'Université de Strasbourg*, May 25-26, 2019, Strasbourg, France.
37. Dresp-Langley, B.; Wandeto, J.M. Unsupervised classification of cell imaging data using the quantization error in a Self-Organizing Map. *Transactions on Computational Science and Computational Intelligence*, H. R. Arabnia et al. (Eds.), Advances in Artificial Intelligence and Applied Computing, Springer-Nature, in the press.
38. Wandeto, J.M.; Nyongesa, H.K.O.; Remond, Y., Dresp-Langley, B. Detection of small changes in medical and random-dot images comparing self-organizing map performance to human detection. *Inform Med Unlocked*, 2017**,** 7, 39-45.
39. Wandeto, J.M.; Nyongesa, H.K.O., Dresp-Langley, B. Detection of smallest changes in complex images comparing self-organizing map and expert performance. 40th European Conference on Visual Perception, Berlin, Germany. *Perception*, 2017, 46(ECVP Abstracts), 166.
40. Wandeto, J.M.; Dresp-Langley, B., Nyongesa, H.K.O. Vision-inspired automatic detection of water-level changes in satellite images: the example of Lake Mead. 41st European Conference on Visual Perception, Trieste, Italy. *Perception*, 2018, 47(ECVP Abstracts), 57.
41. Dresp-Langley, B.; Wandeto, J.M., Nyongesa, H.K.O. Using the quantization error from Self-Organizing Map output for fast detection of critical variations in image time series. In ISTE OpenScience, collection "*From data to decisions*", 2018, London: Wiley & Sons.
42. Wandeto, JM.; Dresp-Langley, B. The quantization error in a Self-Organizing Map as a contrast and colour specific indicator of single-pixel change in large random patterns, *Neural Networks*, 2019, 119, 273-285.
43. Wandeto, J.M., Dresp-Langley, B. Contribution to the Honour of Steve Grossberg's 80th Birthday Special Issue: The quantization error in a Self-Organizing Map as a contrast and colour specific indicator of single-pixel change in large random patterns. *Neural Networks*, 2019, 120, 116–128.
44. Dresp-Langley, B.; Wandeto, J.M. Pixel precise unsupervised detection of viral particle proliferation in cellular imaging data. *Inform Med Unlocked*, 2020, 20, article 100433.
45. Dresp-Langley, B.; Reeves, A. Simultaneous brightness and apparent depth from true colors on grey: Chevreul revisited. *Seeing & Perceiving*, 2012, 25(6), 597-618.
46. Dresp-Langley, B.; Reeves A. Effects of saturation and contrast polarity on the figure-ground organization of color on gray. *Front Psychol*, 2014, 5, article 1136.
47. Dresp-Langley, B.; Reeves, A. Color and Figure-Ground: From Signals to Qualia, In A. Geremek, M. Greenlee, S. Magnussen (Eds.), *Perception Beyond Gestalt: Progress in Vision Research*, 2016, Psychology Press, Routledge, pp. 159-71.
48. Dresp-Langley, B., Reeves A. Color for the perceptual organization of the pictorial plane: Victor Vasarely's legacy to Gestalt psychology. *Heliyon*, 2020, 6(7), article 04375.
49. Bonnet, C., Fauquet A.J.; Estaún Ferrer, S. Reaction times as a measure of uncertainty. *Psicothema*, 2008, 20(1), 43-8.
50. Brown, S.D.; Marley, A.A.; Donkin, C.; Heathcote, A. An integrated model of choices and response times in absolute identification. *Psychol Rev*, 2008, 115(2), 396-425.
51. Ishihara, S. Tests for color-blindness, 1917, Handaya, Tokyo, Hongo Harukicho.

52. Monfouga, M. *Python code for 2AFC forced-choice experiments using contrast patterns*, 2019, available online at: https://pumpkinmarie.github.io/ExperimentalPictureSoftware/, last accessed on 08/01/2021.
53. Dresp-Langley B, Monfouga M. Combining Visual Contrast Information with Sound Can Produce Faster Decisions. *Information*, 2019; *10*, 346.
54. Kohonen, T. *Self-Organizing Maps*. 2001, available online at: http://link.springer.com/10.1007/978-3-642-56927-2, last accessed on 08/01/2021.
55. Kohonen, T. MATLAB Implementations and Applications of the Self-Organizing Map. *Unigrafia Oy*, 2014, Helsinki, Finland.
56. Dresp, B; Fischer, S. Asymmetrical contrast effects induced by luminance and color configurations. *Perception & Psychophysics*, 2001, 63(7), 1262-1270.
57. Dresp-Langley, B. Why the brain knows more than we do: Non-conscious representations and their role in the construction of conscious experience. *Brain Sci.*, 2012, 2, 1–21.
58. Dresp-Langley, B. Generic properties of curvature sensing by vision and touch. *Comput. Math. Methods Med.*, 2013, 634168.
59. Dresp-Langley, B. 2D geometry predicts perceived visual curvature in context-free viewing. *Comput. Intell.Neurosci.*, 2015, 9.
60. Gerbino, W.; Zhang, L. Visual orientation and symmetry detection under affine transformations. *Bull. Psychon. Soc.* 1991, 29, 480.
61. Batmaz, A.U.; de Mathelin, M.; Dresp-Langley, B. Seeing virtual while acting real: Visual display and strategy effects on the time and precision of eye-hand coordination. *PLoS ONE*, 2017, *12*(8).
62. Dresp-Langley, B. Principles of perceptual grouping: Implications for image-guided surgery. *Front. Psychol.*, 2015, *6*, 1565.
63. Martinovic, J.; Jennings, B.J.; Makin, A.D.J.; Bertamini, M.; Angelescu, I. Symmetry perception for patterns defined by color and luminance. *J Vis.*, 2018, 18(8), article 4.
64. Treder, M.S. Behind the Looking-Glass: A Review on Human Symmetry Perception. *Symmetry*, 2010, *2*, 1510-1543.
65. Spillmann, L.; Dresp-Langley, B.; Tseng, C.H. Beyond the classic receptive field: The effect of contextual stimuli, *J. Vis*, 2015, 15, article7.